JOURNAL OF AIRCRAFT
Vol. 46, No. 3, May–June 2009

Pitch Stability Analysis of an Airfoil in Ground Effect

Gerald M. Angle II,* Brian M. O'Hara,† Franz A. Pertl,‡ and James E. Smith§
West Virginia University, Morgantown, West Virginia 26506-6106

DOI: 10.2514/1.31246

The effects of placing a slot through a two-dimensional Wortmann FX 63-137 airfoil in ground effect were examined using computational fluid dynamics. The geometric shape of the slot was varied in three different ways: the width of the slot ($w/c = 0.02$, 0.04, and 0.06), the angle of the slot with respect to the airfoil's chord line ($d = 20$, 30, and 40), and the position of the slot along the chord line, ($x/c = 0.15$, 0.20, and 0.25). In addition, the airfoil was tested at five different angles of attack: −3, 0, 5, 10, and 15 deg. The commercially available software Gambit 2.3.16 was used to create the computational grids. FLUENT 6.2.16 with the renormalized group *k-e* turbulence model was then used to simulate the flow. Pitch stability of the slotted airfoil was examined and results indicated that increasing the angle of attack of the slotted airfoil while in ground effect had a reduced increase in lift when compared with the lift generated by the baseline Wortmann FX 63-137 airfoil. Results also showed that the slot could be used to reduce center-of-pressure movement along the chord of the airfoil for the range of angles of attack investigated, thus improving the overall pitch stability of the airfoil. The slot geometry that produced a minimal center-of-pressure fluctuation was located at 20% of the chord length from the leading edge with a width of 2% and an angle of 20 deg between the slot and a line normal to the chord line.

Nomenclature

α	=	angle of attack
C_l	=	coefficient of lift
$C_{l\infty}$	=	coefficient of lift out of ground effect
c	=	chord length of the airfoil
d	=	slot angle
F_y	=	force in the vertical direction
H, h	=	height of the lowest point on a flat plate
h_{le}	=	height of the leading edge above the ground
h_{te}	=	height of the trailing edge above the ground
M_{LE}	=	moment about the leading edge
U	=	horizontal velocity
w	=	slot width
x	=	slot distance from the leading edge
x_{cp}	=	center-of-pressure location
y^+	=	nondimensional distance
ρ	=	density of air
Δx_{cp}	=	change in the center-of-pressure location

Introduction

WHEN a lifting device such as an airfoil travels steadily in close proximity to a nonporous medium such as water, sand, ice, or land, the effect felt by the lifting device is called ground effect (Rozhdestvensky [1]). For clarification, the term *ground* as described in this paper applies to any nonporous material that an aircraft may come in close proximity to during flight. The benefits and detriments of ground effect and instabilities resulting from it have been well documented in previous literature by Rozhdestvenky [1], Plotkin and Dodbele [2], Ahamed [3], and Dragos [4], and so a full review will not be presented.

Pitch instability of a wing in ground-effect aircraft can be especially problematic. If the aircraft pitches up or down too much, ground contact or aerodynamic stall could occur with disastrous results. It is proposed that placing a slot through an airfoil could decrease pitch instabilities. For this study, a Wortmann FX-63-137 airfoil was used. Figure 1 shows this airfoil with the slot in place. The slot was defined by three characteristics: the width of the slot ($w/c = 0.02$, 0.04, and 0.06), the angle of the slot with respect to normal to the chord line ($d = 20$, 30, and 40 deg), and the position of the slot along the chord line from the leading edge to center of the slot ($x/c = 0.15$, 0.20, and 0.25). Figure 2 illustrates these dimensions, which were then varied to create 15 different slotted airfoils.

Each airfoil was tested using computational fluid dynamics (CFD) which has been shown to accurately predict airfoil performance in ground effect, according to Hsiun and Chen [5]. However, a passive slotted airfoil can be challenging for CFD simulations, particularly in the areas around the slot in which flow separation, circulation, and turbulence can arise due to the existence of the slot. Through careful model construction, it is possible for CFD to provide physically realistic results for complex geometry such as the slotted airfoil (Anderson [6]).

When conducting a CFD analysis, it is essential to confirm that the results accurately represent the physical phenomenon. Experimental and analytical results of a slotted airfoil were not available; instead, computational methods of a known flat-plate airfoil were used to validate and compare with the ground-effect analytical models.

Received 26 March 2007; revision received 13 July 2007; accepted for publication 13 July 2007.

*Postdoctoral Fellow, Center for Industrial Research Applications, Mechanical and Aerospace Engineering, College of Engineering and Mineral Resources, P.O. Box 6106; gangle@mix.wvu.edu. Member AIAA.

†Graduate Research Assistant, Center for Industrial Research Applications, Mechanical and Aerospace Engineering, College of Engineering and Mineral Resources, P.O. Box 6106; bohara@mix.wvu.edu. Student Member AIAA.

‡Program Coordinator, Center for Industrial Research Applications, Mechanical and Aerospace Engineering, College of Engineering and Mineral Resources, P.O. Box 6106; franz.pertl@mail.wvu.edu.

§Professor and Director, Center for Industrial Research Applications, Mechanical and Aerospace Engineering, College of Engineering and Mineral Resources, P.O. Box 6106; james.smith@mail.wvu.edu. Member AIAA.

Flat-Plate Analysis

Analytical Models: Flat Plate

The analytical model for a flat plate in ground effect was used to validate the computational methods used in this evaluation. The analytical model, presented by Coulliette and Plotkin [7], compares the lift of a zero-thickness flat plate in ground effect with the lift out of ground effect. Equation (1) shows the relation between the coefficient of lift in ground effect and the coefficient of lift out of ground effect. The analytical model of Eq. (1) was developed for incompressible irrotational flow using a no-slip boundary condition:

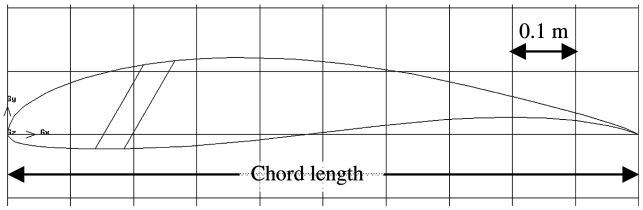

Fig. 1 Wortmann FX63-137 airfoil with slot.

$$\frac{C_l}{C_{l_\infty}} = 1 - \frac{c}{2 \cdot H}\sin\alpha + \frac{c^2}{16 \cdot H^2}(1 + 3 \cdot \sin^2\alpha) \tag{1}$$

An additional model, also presented by Coulliette and Plotkin [7], used Tuck's [8] small height approximation. This relationship was developed for a ground height similar to the change in height of the flat plate due to the angle of attack. It provides an approximation for the coefficient of lift. Equation (2) from Coulliette and Plotkin [7] predicts the coefficient of lift based on the height at the trailing edge and the height at the leading edge of the flat plate along with the angle of attack:

$$C_l = \cos\alpha\left(1 - \frac{h_{\text{te}}}{h_{\text{le}}}\right) \tag{2}$$

Computational-Grid Setup: Flat Plate

Two geometries were created for the flat-plate airfoil analysis. The first was a flat plate in ground effect at an h/c of 0.25, where h is the minimum height of the airfoil. The second geometry was a flat plate out of ground effect to allow for comparison with the analytical models. The grid of the flat plate in ground effect was constructed of a structured mesh immediately around a zero-thickness plate. Outside of the structured area, unstructured triangular cells were used with a growth rate of 1.05 extending from the structured mesh with a maximum size of 0.3, as shown in Fig. 3. A velocity inlet was placed 9 chord lengths upstream, a pressure outlet was placed 9 chord lengths downstream, and a stationary wall was placed 10 chord lengths above the flat plate. A moving wall was placed one-fourth of the chord length below the lowest point of the plate. One thousand grid points were created on the flat plate. The total number of cells for the flat-plate grid was approximately 250,000 cells.

The grids for the flat plate out of ground effect relocated the moving wall to 10 chord lengths underneath the flat plate. The number of cells in the out-of-ground-effect flat-plate grid was approximately 300,000 cells.

Boundary Conditions

The commercial CFD software FLUENT 6.2.16 allows for the creation of various types of boundaries. The same boundary conditions were used for each grid: the left side of the grid was set as a uniform velocity inlet, which resulted in a Reynolds number of 1.25×10^6 for every case, and the right side of the grid was set as a pressure outlet of 0 Pa gauge pressure. The bottom of the grid was set as a translational moving wall for which the speed matched the velocity inlet from left to right and a no-slip shear condition was applied to the moving wall. The rest of the boundaries, the top wall and airfoil surfaces, were set as stationary no-slip walls. The simulated fluid was standard air at 101,325 Pa at a temperature of 288 K, and gravity was applied at -9.81 m/s^2 in the vertical direction.

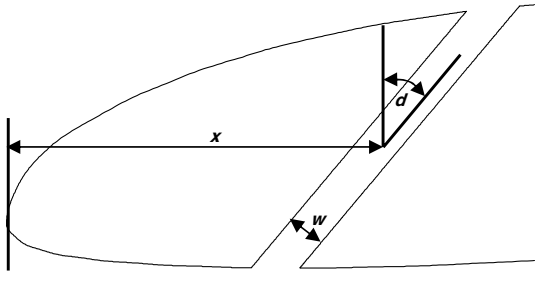

Fig. 2 Slot-dimensional parameters.

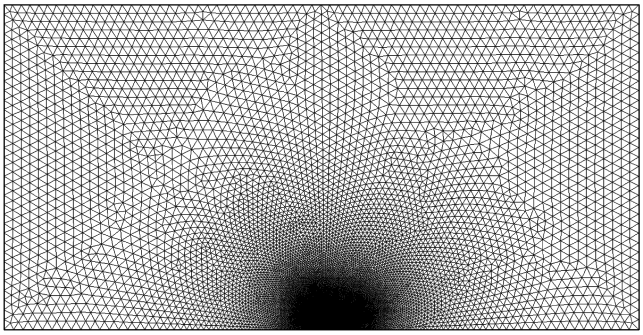

Fig. 3 View of the entire flat-plate grid.

Solution Procedure

The 2-D steady segregated solver was used in the computational setup with the node-based gradient option selected, because the grid had areas of both structured and unstructured cells. Two solutions were computed for each case; a preliminary solution was found using first-order discretization and the laminar viscous model. The preliminary solution was then used to initialize the second and final solution, which used the two-equation renormalized group k-e turbulence model with enhanced wall treatment. This turbulence model was selected because it has been found previously to yield good results for cases that require a fine-grid structure, good prediction of flow separation, and turbulence modeling (O'Hara et al. [9]).

After the final solution was obtained for each case, the lift, drag, and pitching moment imposed on the airfoil were extrapolated using the computational software. These forces were used to calculate the coefficient of lift using Eq. (3). Equation (4) was used to calculate x_{cp} with the moment taken about the leading edge of the airfoil and the force in the y direction. The change in the center-of-pressure location was found by determining the maximum difference between the x_{cp} found at various angles of attack:

$$C_l = \frac{F_y}{\frac{1}{2}\rho U^2 A} \tag{3}$$

$$x_{\text{cp}} = \frac{M_{\text{LE}}}{F_y} \tag{4}$$

Results: Flat Plate

As expected, the flat-plate's coefficient of lift had a larger magnitude in ground effect than out of ground effect. Figure 4 shows that the flat plate has close to 0 lift at an angle of attack of 0 deg. When the plate was out of ground effect, a nearly linear relationship was found between the coefficient of lift and the angle of attack. When in ground effect, changes in the angle of attack had a greater influence on the lift created. These trends agree with the analytical models presented by Coulliette and Plotkin [7]. Figure 4 shows the comparison of the in-ground-effect prediction [Eq. (1)] applied to out-of-ground-effect data presented by Anderson [10] and the computational results for both in and out of ground effect.

Figure 4 shows that the computational model overpredicts the solution at high angles of attack for the flat plate. The analytical model from Coulliette and Plotkin [7] [Eq. (2)] slightly underpredicts the lift when compared with the experimental values shown by Anderson [10]. The enhancement of lift due to ground effect,

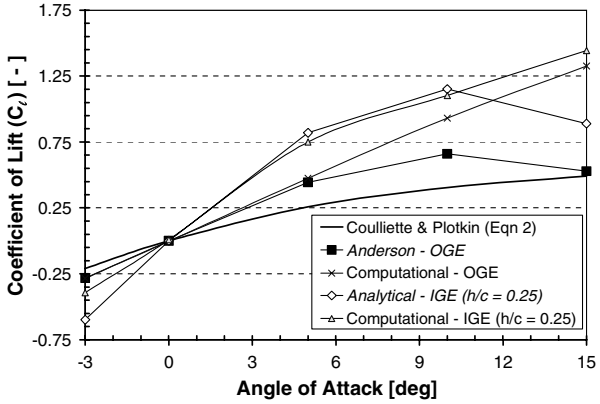

Fig. 4 Comparison of C_l and $C_{l\infty}$ for the analytical (Coulliette and Plotkin [7]) and computational solutions of the flat plate to data presented by Anderson [10] (OGE denotes out of ground effect and IGE denotes in ground effect).

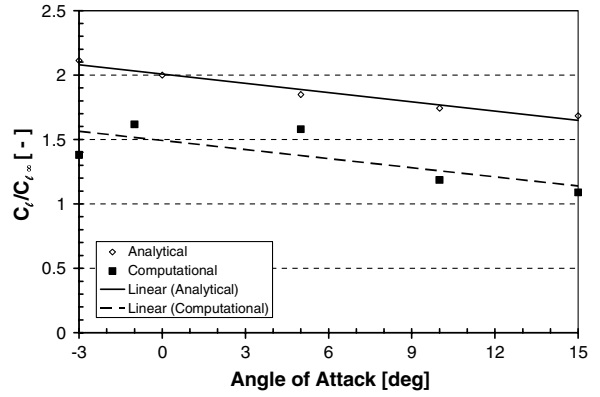

Fig. 5 Comparison of analytical [Eq. (1)] and computational methods for predicting flat-plate coefficient of lift enhancement in ground effect.

$C_l/C_{l\infty}$, shown in Fig. 5, was underpredicted by the computational analysis when compared with the analytical method of Eq. (1). These differences in the C_l for the computational and analytical models can be explained by examining the assumptions made during the analytical solution and vector plots of the CFD solution. The analytical models predict the flow around a flat plate based on laminar irrotational flow relationships. Figure 6 shows the CFD-predicted airflow over a zero-thickness flat plate at an angle of attack of 5 deg. A separation bubble is present over half of the chord length on the upper surface of the plate. So the CFD and analytical models of this complex flow scenario can both be considered to be approximately valid within specific ranges in angle of attack. The computationally determined center-of-pressure location for the flat-plate airfoil is shown in Fig. 7, in which the change in the center of pressure with angle of attack approximately doubles due to the presence of the ground. This increased travel of the center of pressure illustrates the difficulty of maintaining controlled flight in ground effect without the use of flight computers or some compensating system for reducing this center-of-pressure travel.

Like many approximate solutions, experimental data is needed for comparison. In the absence of this data, the data presented by Anderson [10] is assumed to be the most accurate solution. From Fig. 4 it is shown that the computational solution can adequately predict the lift coefficient of a flat-plate airfoil up to an angle of attack of 5 deg. When the plate is in ground effect, at a height equal to a quarter of the chord length, CFD adequately predicts the lift coefficient up to an angle of 10 deg. Hence, similar computational techniques can be used with reasonable confidence to analyze a Wortmann FX 63-137 airfoil in ground effect.

Slotted Wortmann FX 63-137 Airfoil Analysis

Computational-Grid Setup: Wortmann Airfoil

According to Moran [11], the creation of a quality computational grid is particularly important to ensure accurate results when the flow is mostly unknown. The more complex slotted-airfoil grid, although similar to the flat-plate grids, were constructed to reflect these attributes. Figure 8 shows the 2-D cross section of the modified FX 63-137 airfoil geometry along with the surrounding boundaries. Like the flat plate in-ground-effect grid, the moving ground plane was placed under the airfoil at a distance of one-fourth of the chord length. The surrounding boundaries, velocity inlet, stationary wall, and pressure outlet were placed at the same distances from the airfoil as those of the flat-plate study, as shown in Fig. 8.

The no-slip walls of the airfoil surfaces had a high density of grid points. The number of grid points was set such that all of the necessary viscous effects could be accurately modeled by the solver. The y^+ value was used to initially predict the grid quality. This quantity is a measurement of the normal spacing needed to capture the viscous effects next to a solid boundary. The airfoil boundaries had 1320 grid points around its surface, excluding the grid points inside the slot. This allowed the y^+ value to stay below 5, as recommended by FLUENT documentation [12].

A slightly different grid was created for each variation of the slot dimensions. The cell spacing throughout each grid was kept as constant as possible. The number of grid points around and under the airfoil remained equal for each grid. The basic structure of the entire mesh also remained uniform. Figure 9 shows the structured quadrilateral cells that are in the form of a large U-shaped grid around

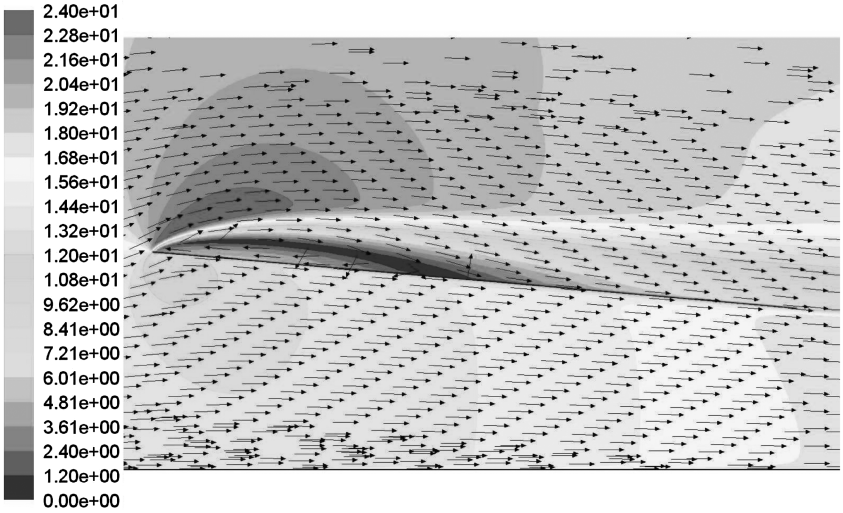

Fig. 6 Velocity vector contour plot of flat plate in ground effect (meters/second).

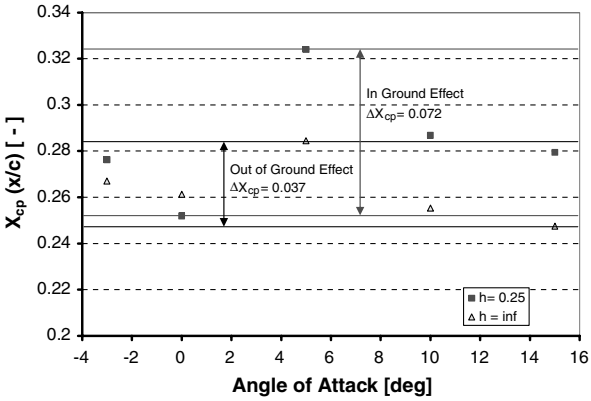

Fig. 7 Center-of-pressure location of a flat-plate airfoil.

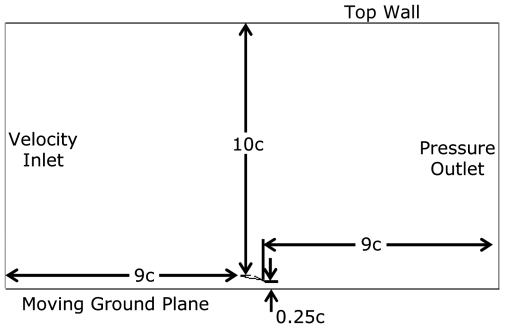

Fig. 8 Dimensions of grid with boundaries.

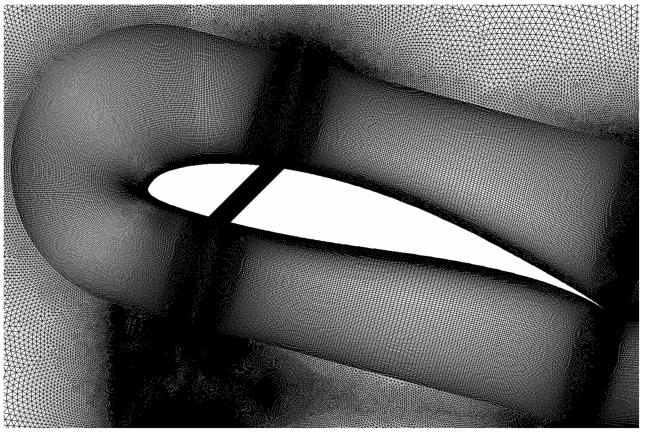

Fig. 9 Close-up of slotted-airfoil grid.

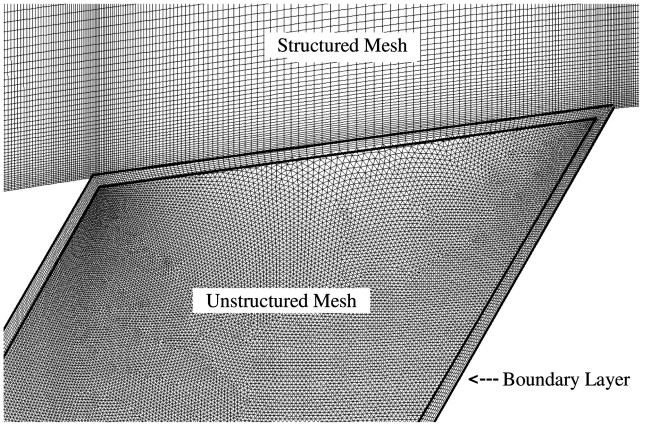

Fig. 10 Grid within slotted-airfoil slot.

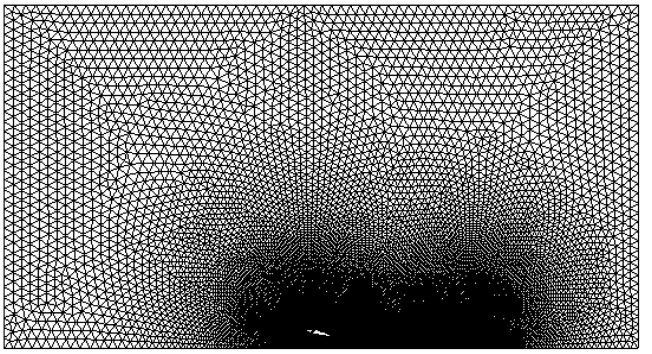

Fig. 11 View of the entire slotted-airfoil grid.

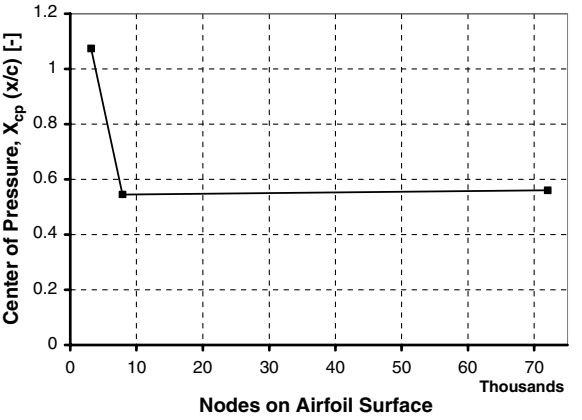

Fig. 12 Grid independence of the center-of-pressure location.

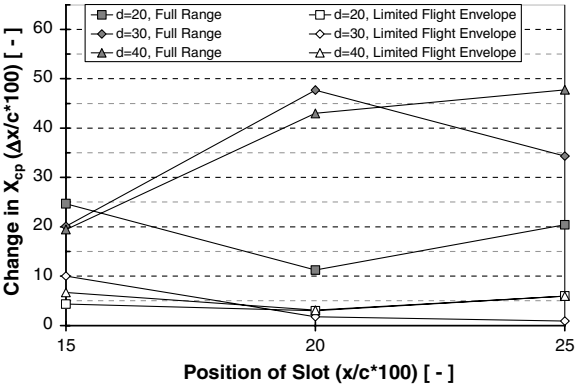

Fig. 13 Effect of varying slot position for the full and limited angle-of-attack ranges.

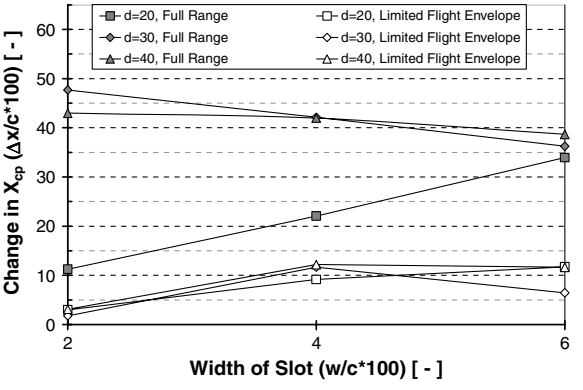

Fig. 14 Effect of varying slot width for the full and limited angle-of-attack ranges.

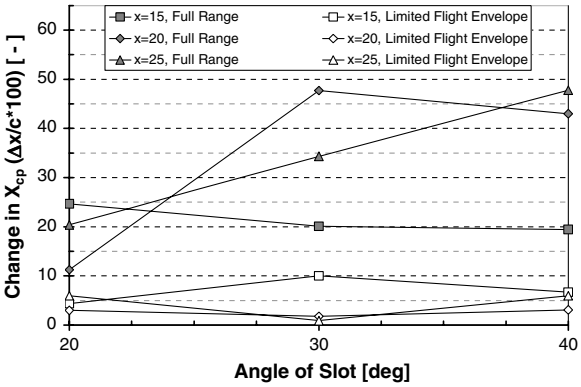

Fig. 15 Effect of varying slot angle for the full and limited angle-of-attack ranges.

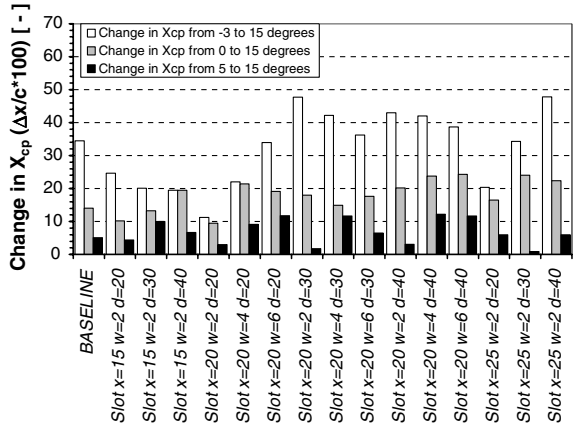

Fig. 16 Comparison of Δx_{cp} for every case for three different α ranges.

the airfoil. Directly downstream of the airfoil, there was a block of quadrilateral structured cells for 4 chord lengths downstream of the airfoil's trailing edge. The most critical area within the slot was composed of high-density triangular cells surrounded by a 5-cell-thick boundary layer of quadrilateral cells. Figure 10 shows a close-up view of the upper slot area in which the boundary layers were used to smooth out the transition regions between the unstructured slot and the structured area around the airfoil. The remainder of the grid was composed of unstructured triangular cells that extended from the structured edges at a growth rate of 1.05 with a maximum grid size of 0.3, shown in Fig. 11.

Each grid used the same basic structure as described previously, but there were differences depending on the geometry of the slot and the angle of attack of the airfoil. In an effort to keep the grid spacing equal for each geometry, differences in the number of cells were necessary. Grid spacing within the slot was kept nearly constant for every variation. Grid spacing under the airfoil was also nearly equal for each angle of attack. Because the area underneath the airfoil changed depending on the angle of attack, the number of cells changed accordingly.

A grid independence check was completed by adjusting the number of grid points on the surface of the airfoil and adjacent geometries. The initial grid contained 7892 grid points, which was reduced by approximately half, resulting in the coarse grid, which contained 3140 points on the surface. A fine grid was created by increasing the number of grid points by an order of magnitude to 72,025 points. Figure 12 compares the resulting center-of-pressure location from the initial grids. From this grid independence evaluation, it was determined that the airfoil should have approximately 8000 grid points on its surface to obtain reasonable results with the shortest required computational time.

Boundary Conditions: Wortmann Airfoil

The same basic boundary conditions were used for the Wortmann FX 63-137 airfoil cases as those used for the flat-plate analysis. The velocity inlet was set to produce a Reynolds number of 1.25×10^6, and the moving ground plane was set at the corresponding velocity. The pressure outlet was set at 0 Pa gauge pressure. The main difference between the flat-plate and airfoil boundary conditions is the creation of the passive slot in the airfoil. The slot's geometry, as defined by the location of its center, the angle of the slot, and its width, required the surface of the airfoil to have differing boundary conditions. Thus, the surface was partitioned such that the edge of the slot was an interior face, allowing for the calculation of the airflow through the slot. The remaining surfaces of the airfoil, including the linear sides of the slot, were set as walls with a no-slip condition applied.

Solution Procedure: Wortmann Airfoil

The solution method to determine the lift coefficient and center-of-pressure location for the slotted airfoil was the same as that used for the flat plate. The change in the center-of-pressure location was determined for several ranges of angle of attack. The full range in angle of attack was from -3 to 15 deg, which was further refined to a range of 0 to 15 deg, as well as the range from 5 to 15 deg, which is referred to as the limited flight envelope. These different ranges were useful in determining the pitch characteristics of the slotted airfoils.

Results: Wortmann Airfoil

Because the slotted airfoils do not have a comparable analytical model or historical experimental data for comparison, the flat-plate analysis was used as validation of the computational methodology and meshing scheme. The results with slot parameters of slot width $w/c = 0.02$, 0.04, and 0.06; slot angle with regard to the chord line of $d = 20$ deg, 30, and 40 deg; and the slot position along the chord line from the leading edge to the slot center of $x/c = 0.15$, 0.20, and

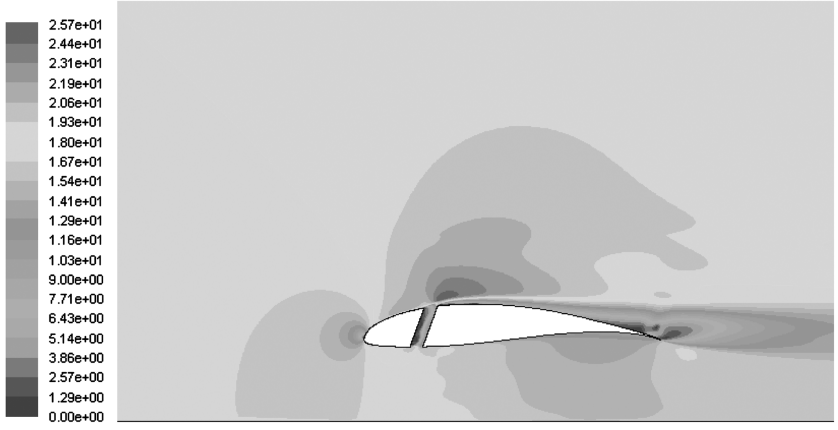

Fig. 17 Velocity contour of FX 63-137 slotted airfoil at 0 deg angle of attack with slot ($x/c = 0.20$, $w/c = 0.04$, $d = 20$ deg).

0.25 are compared with a computational baseline Wortmann FX 63-137 airfoil model.

For the baseline and every slotted-airfoil case, the change in the center-of-pressure location was determined for a range of angles of attack (−3, 0, 5, 10, and 15 deg). Figures 13–15 show how each of the three slot parameters affected Δx_{cp}. Each graph shows Δx_{cp} for the previously defined ranges of angle of attack: the full range of −3 to 15 deg and the limited flight envelope of 5 to 15 deg. For the baseline airfoil, Δx_{cp} was 34.5%c for the full angle-of-attack range, and 5.1%c for the limited flight envelope. Figure 13 shows the variation in the center-of-pressure location for the slotted airfoil with a slot at different positions along the chord length (15, 20, and 25% of c). The smallest Δx_{cp} was found to be 11.2%c for the full range of angles of attack, a slot position of $x/c = 0.20$, and a uniform slot width of $w/c = 0.02$.

Figure 14 shows the effect of changing the slot width on Δx_{cp} when the position of the slot is held constant at $x/c = 0.20$. A slot width of $w/c = 0.02$ resulted in the smallest change in X_{cp} of 11.2%c. Figure 15 shows how the third slot parameter, the slot angle with respect to the chord normal, affected the change in the center-of-pressure location. The lowest Δx_{cp} occurred at a slot angle of 30 deg. The results show low sensitivity of Δx_{cp} to changes in slot angle, especially for the flight-envelope angle-of-attack range used in this analysis.

From the data presented in Figs. 13–15, it would seem reasonable to expect the smallest Δx_{cp} to be found for an airfoil slot with parameters $x/c = 0.20$, $w/c = 0.02$, and $d = 30$ deg. Directly comparing the change in the center-of-pressure location as in Fig. 16 supports this assessment for the limited flight envelope. However, this case also had a larger Δx_{cp} when considering the full range of angles of attack. The smallest Δx_{cp} for the limited flight envelope is 0.9% c, which occurred for slot parameters $x/c = 0.25$, $w/c = 0.2$, and $d = 30$ deg. Figure 17 shows the velocity contour around the slot ($x/c = 0.2$, $w/c = 0.04$, and $d = 20$ deg), where it can be seen that at low angles of attack, there is little airflow through the passive unsealed slot.

The use of such a passive pitch control slot also influences the lift characteristics of the airfoil. The coefficient of lift for the slotted airfoils with x/c of 0.15, 0.20, and 0.25 are shown in Figs. 18–20, respectively, with $w/c = 0.02$ held fixed. Adjusting the slot width w/c has little effect on the lift coefficient, as seen in Fig. 21. The two slot setups that resulted in the smallest center-of-pressure travel over the full angle-of-attack range alter the lift coefficient differently, as shown in Fig. 22. Thus, the slot case ($x/c = 0.2$, $w/c = 0.2$, and $d = 20$ deg) may be the most reliable option, because it performs well for the complete angle-of-attack range in both lift and center-of-pressure travel.

Recommendations

The potential increase in pitch stability control through the use of a passive slotted airfoil was shown computationally in this research and needs to be experimentally validated. The authors are currently

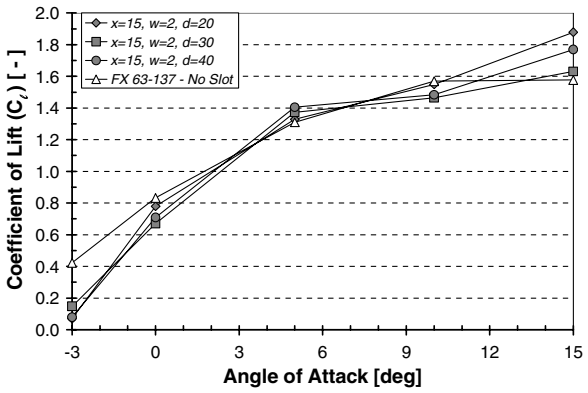

Fig. 18 Coefficient of lift for slot position $x/c = 0.15$.

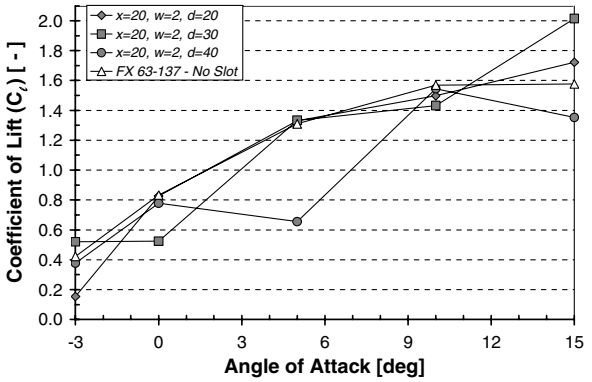

Fig. 19 Coefficient of lift for slot position $x/c = 0.20$.

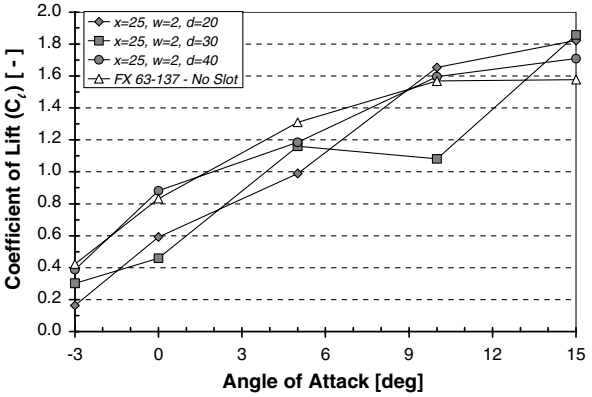

Fig. 20 Coefficient of lift for slot position $x/c = 0.25$.

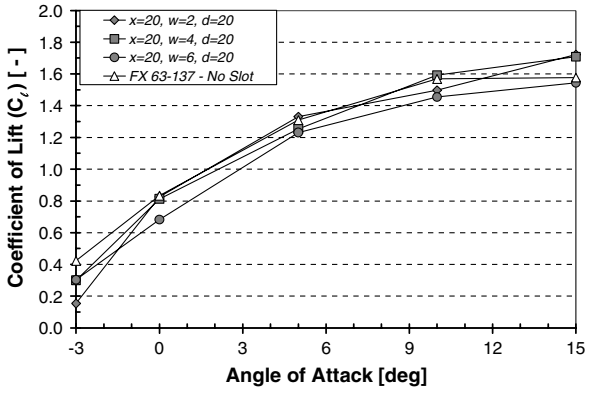

Fig. 21 Coefficient of lift for varying slot widths.

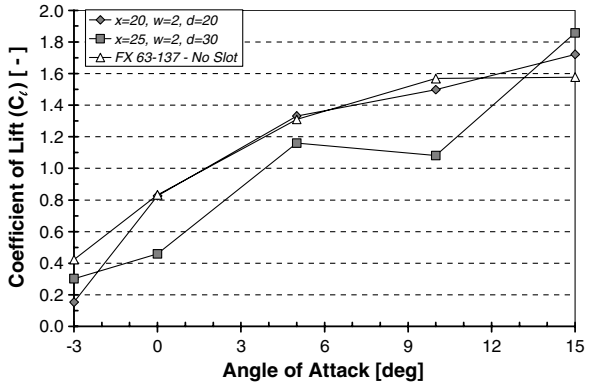

Fig. 22 Coefficient of lift for two selected slotted airfoils with small Δx_{cp}.

developing a series of experimental test models and a test plan to conduct experimental analysis of pitch stability for a slotted airfoil in ground-effect flight. This experimental validation is highly recommended before further computational analysis is conducted of more complex slot profiles. The future complex slots could include slots that have any shape that can be structurally managed within a wing, such as converging, diverging, or arced. Other airfoil parameters that should be eventually investigated in conjunction with the passive slots are camber, thickness, and the effects on control surface performance. Other potential design variations could include multiple slots in a wing, allowing the designer additional control over how the wing controls the pitching moment fluctuation that is typical of ground-effect flight.

Conclusions

For moderate angles of attack of 0 to 10 deg, the flat-plate computational models adequately predict the coefficient of lift in and out of ground effect, but diverge away from the data from Anderson [10] outside of this range, where the corresponding increase in lift can be analytically predicted in ground effect. This reasonable agreement over the moderate angles of attack allowed the modeling and simulation techniques to be applied with reasonable confidence when analyzing the addition of a passive slot in an airfoil to alleviate the considerable pitching moment changes that are typical of ground-effect flight.

It was found during this research that a passive slot in an airfoil can be used to considerably limit the center-of-pressure travel of an airfoil in ground effect. Two of the slots investigated in this research were found to limit the center-of-pressure travel to approximately 10% of the chord length, more than a threefold reduction from the 34% for the unaltered airfoil. The slot parameters that resulted in this reduction were found to be $x/c = 0.20$, $w/c = 0.02$, and $d = 20$ deg. The slotted-airfoil lift coefficient was no less than 94% of the unslotted-airfoil case over an angle-of-attack range from 0 to 15 deg. This shows the potential for a passive slot in improving the pitch stability of an airfoil in ground effect with minimal loss of lift, even at angles of attack approaching stall.

References

[1] Rozhdestvensky, K. V., *Aerodynamics of a Lifting System in Extreme Ground Effect*, Springer–Verlag, Berlin, 2000, Chaps. 1–3, 9.

[2] Plotkin, A., and Dodbele, S., "Slender Wing in Ground Effect," *AIAA Journal*, Vol. 26, No. 4, Apr. 1988, pp. 493–494. doi:10.2514/3.9920

[3] Ahamed, M. R., "Aerodynamics of a NACA4412 Airfoil in Ground Effect," *AIAA Journal*, Vol. 45, No. 1, Jan 2007, pp. 37–47. doi:10.2514/1.23872

[4] Dragos, L., "Numerical Solution of the Equation for a Thin Airfoil in Ground Effect," *AIAA Journal*, Vol. 28, No. 12, December 1990, pp. 2132–2134. doi:10.2514/3.10532

[5] Hsiun, C., and Chen, C., "Aerodynamic Characteristics of a Two-Dimensional Airfoil with Ground Effect," *Journal of Aircraft*, Vol. 33, No. 2, Apr. 1996, pp. 386–392. doi:10.2514/3.46949

[6] Anderson, J., *Computational Fluid Dynamics The Basics with Applications*, McGraw–Hill, New York, 1995.

[7] Coulliette, C., and Plotkin, A., "Aerofoil Ground Effect Revisited," *The Aeronautical Journal*, Vol 100, No. 992, Feb. 1996, pp. 65–74.

[8] Tuck, E. O., "Steady Flow and Static Stability of Airfoils in Extreme Ground Effect," *Journal of Engineering Mathematics*, Vol. 15, No. 2, 1981, pp. 89–102. doi:10.1007/BF00052513

[9] O'Hara, B. M., Angle, G. M., II, Riba, C. A., Huebsch, W. W., and Smith, J. E., "Continued Computational Investigation into Circulation Control for the V-22 Osprey Download Reduction," Society of Automotive Engineers TP 05IPLC-26, Aug. 2005.

[10] Anderson, J., *Fundamentals of Aerodynamics*, 2nd Ed., McGraw–Hill, New York, 1991.

[11] Moran, J., *An Introduction to Theoretical and Computational Aerodynamics*, Dover, Mineola, NY, 1984.

[12] *FLUENT 6.2 User's Guide*, Fluent, Inc., Lebanon, NH, 2005, http://www.fluentusers.com/fluent/doc/doc_f.htm [retrieved 2009].